Urinary bladder segmentation in CT urography (CTU) using CLASS

Lubomir Hadjiiski,[a)] Heang-Ping Chan, Richard H. Cohan, Elaine M. Caoili, Yuen Law, Kenny Cha, Chuan Zhou, and Jun Wei
Department of Radiology, the University of Michigan, Ann Arbor, Michigan 48109-0904

(Received 18 April 2013; revised 13 September 2013; accepted for publication 16 September 2013; published 10 October 2013)

Purpose: The authors are developing a computerized system for bladder segmentation on CTU, as a critical component for computer aided diagnosis of bladder cancer.
Methods: A challenge for bladder segmentation is the presence of regions without contrast (NC) and filled with intravenous contrast (C). The authors have designed a Conjoint Level set Analysis and Segmentation System (CLASS) specifically for this application. CLASS performs a series of image processing tasks: preprocessing, initial segmentation, 3D and 2D level set segmentation, and postprocessing, designed according to the characteristics of the bladder in CTU. The NC and the C regions of the bladder were segmented separately in CLASS. The final contour is obtained in the postprocessing stage by the union of the NC and C contours. With Institutional Review Board (IRB) approval, the authors retrospectively collected 81 CTU scans, in which 40 bladders contained lesions, 26 contained diffuse wall thickening, and 15 were considered to be normal. The bladders were segmented by CLASS and the performance was assessed by rating the quality of the contours on a 10-point scale (1 = "very poor," 5 = "fair," 10 = "perfect"). For 30 bladders, 3D hand-segmented contours were obtained and the segmentation accuracy of CLASS was evaluated and compared to that of a single level set method in terms of the average minimum distance, average volume intersection ratio, average volume error and Jaccard index.
Results: Of the 81 bladders, the average quality rating for CLASS was 6.5 ± 1.3. Thirty nine bladders were given quality ratings of 7 or above. Only five bladders had ratings under 5. The average minimum distance, average volume intersection ratio, average volume error, and average Jaccard index for CLASS were 3.5 ± 1.3 mm, (79.0 ± 8.2)%, (16.1 ± 16.3)%, and (75.7 ± 8.4)%, respectively, and for the single level set method were 5.2 ± 2.6 mm, (78.8 ± 16.3)%, (8.3 ± 33.1)%, (71.0 ± 15.4)%, respectively.
Conclusions: The results demonstrate the potential of CLASS for segmentation of the bladder.
 [http://dx.doi.org/10.1118/1.4823792]

Key words: computer-aided diagnosis, CT urography, segmentation, level set, bladder, malignancy

1. INTRODUCTION

Bladder cancer produces substantial morbidity and mortality among both men and women. It causes 14 880 deaths per year in the United States.[1] If bladder cancers are detected and treated early, patient survival is high.[1] Early diagnosis and treatment improves morbidity, mortality, and their attendant costs, compared to diagnosis at a later, more symptomatic stage at which time muscular invasion and/or metastasis may be present. Although early detection of bladder cancers is important, currently only about 75% are detected before they have become invasive and/or metastatic.

Multidetector row CT (MDCT) urography is a promising imaging modality for evaluation of urothelial neoplasms,[2–5] which offers the distinct advantage of providing essentially complete imaging of the urinary tract in a single study. CT urography (CTU), therefore, may spare the patient the considerable effort of undergoing a potentially large number of alternative imaging studies [intravenous pyelogram (IVP), ultrasound, conventional abdominal CT, and even MRI], thereby reducing health care costs.

Preliminary studies[6] have demonstrated that CTU may have superior sensitivity to other imaging studies in detecting urinary tract lesions, especially urothelial neoplasms, that are very small (2–3 mm in diameter) compared with all available alternative imaging studies. In fact, CTU can occasionally detect bladder lesions missed by cystoscopy, a procedure which has been traditionally considered to be the "gold standard" for nonsurgical diagnosis of bladder abnormalities.

The interpretation of a CTU study demands careful image analysis, which often requires extensive time for interpretation. On average, usually, at least 300 slices are generated for each CTU scan at a slice interval of 1.25 mm (range: 200–600 slices). The interpreting radiologists have to visually track the upper and lower urinary tracts, look for lesions that may be quite small in size, and frequently need to adjust window settings and use zooming on a display workstation to improve visualization. The possibility that multiple lesions may be present (since some patients have multifocal tumors) requires that the radiologists pay close attention throughout the urinary tract. Despite the improved sensitivity of CTU in assessment of the urothelium, substantial variability exists among radiologists in detection of bladder cancer in CTU, with reported sensitivities ranging from 59% to 92%.[7,8]

Additionally, in any individual CTU scan many different urinary tract findings may be present. Not only must the

interpreting radiologist spend extensive time and effort identifying these findings, but he or she must also then determine how likely each of the findings is to represent a urothelial neoplasm. Any technique that can assist the radiologist in identifying areas of the urinary tract that may contain urothelial neoplasms will be useful.

With the continuing increased demands on radiologists' workloads, the chance for oversight of subtle lesions may not be negligible. Computer-aided detection (CAD) might play an important role in the interpretation of CTU, by serving as an adjunct for the radiologist. We are developing a CAD system for detection of bladder cancer in CTU. A critical component of such CAD system is the accurate segmentation of the bladder from the surrounding anatomical structures in order to define the search space and analyze the bladder wall.

Li *et al.*[9] and Duan *et al.*[10,11] automatically segmented the bladder wall and then analyzed it for suspected lesions on magnetic resonance (MR) cystography in six patients. In a different study Duan *et al.*[12] proposed an adaptive window-setting scheme for segmentation of bladder inner wall and tumor surface on MR scans from ten patients. Song *et al.*[13] proposed a method for globally optimal surface segmentation of multiple mutually interacting objects on CT—the bladder and the prostate, using a 3D graph-theoretic approach. They used 21 CT scans for evaluation of the approach. Chai *et al.*[14,15] developed a statistical-shape-based segmentation approach to segment 23 bladders on CT. They also developed a voxel-based finite element model for the prediction of bladder deformation on 10 MRI scans. Hadjiiski *et al.*[16,17] reported preliminary results for bladder segmentation in CTU scans of 15 and 70 patients using active contour models and level sets evaluated, respectively. The segmentation of bladder in CTU is challenging. Some bladders are fully or partially opacified with intravenous (IV) contrast material and some are not opacified. The boundaries between the bladder and the adjacent normal tissues have very low contrast. The bladders often have different shapes and different sizes.

The purpose of this study is to develop a task-based computerized system for bladder segmentation in CTU and to evaluate its segmentation accuracy.

2. MATERIALS AND METHODS

An example of a 3D reconstruction of the urinary tract using CTU is illustrated in Fig. 1(a). The bladder is visible in the 3D volume. An axial CTU slice of the same case with the bladder partially filled with IV contrast material is shown in Fig. 1(b). A malignant lesion is identified in the contrast-enhanced portion of the bladder and it is also visible in the 3D volume in Fig. 1(a) (bold white arrow). The presence of a large lesion near the bladder wall in the area filled with IV contrast material may be challenging for bladder segmentation because of the large edge gradients resulting from the substantial differences in intensity between the lesion boundary and the IV contrast material. These large edge gradients may stop the segmentation procedure prematurely.

2.A. Bladder segmentation using CLASS

Region of interests (ROIs) on a CTU slice containing the bladder from different cases are shown in Figs. 2 and 3. The bladders are partially filled with IV contrast material and a malignant lesion is present within the opacified lower part of the bladder in Fig. 2. In comparison, a malignant lesion is present within the nonopacified upper part of the bladder in Fig. 3. A challenge for bladder segmentation is the presence of two distinct areas that have very different attenuation values: an area filled with IV contrast material and an area without contrast material (Figs. 2 and 3).

We are developing a new segmentation package, specifically designed based on the characteristics of the bladder in CTU images, which we refer to as the Conjoint Level set Analysis and Segmentation System (CLASS). An introduction of CLASS with preliminary qualitative evaluation was presented previously.[17] In the current study, our focus is on

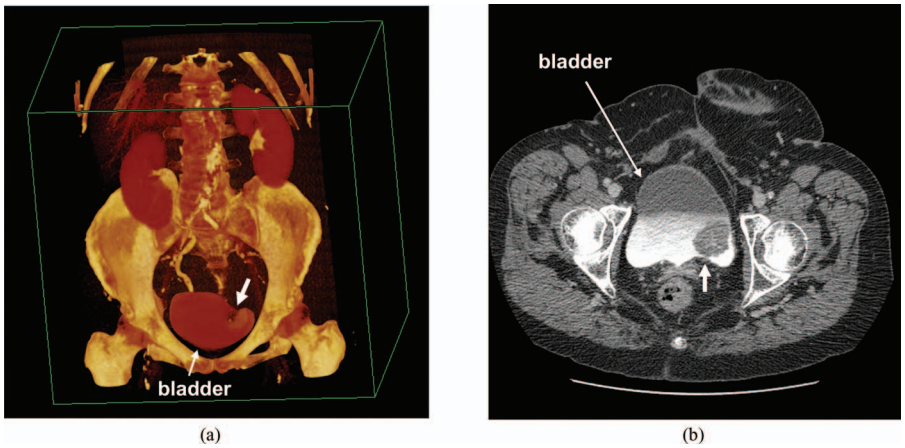

FIG. 1. CTU scan. (a) Volume rendered image from the CTU scan. The bladder is visible in the 3D volume. A malignant lesion is identified and marked by the bold white arrow. (b) Axial slice of the CTU scan from Fig. 1(a) showing the bladder partially filled with IV contrast material. The malignant lesion is identified in the contrast enhanced part of the bladder (bold white arrow).

FIG. 2. ROI containing a bladder partially filled with IV contrast material. A malignant lesion is present in the contrast enhanced part of the bladder (pointed by a white arrow).

the quantitative assessment of the performance of CLASS, comparing its segmentation accuracy to radiologist's manual outlines of the 3D volumes, in addition to their qualitative visual judgment on an enlarged data set. Furthermore, we compared the CLASS performance to that of the open source ITK-SNAP method[18] in terms of a number of quantitative measures.

CLASS consists of four stages: (1) preprocessing and initial segmentation, (2) 3D level set segmentation, (3) 2D level set segmentation, and (4) postprocessing. The block diagram of CLASS is presented in Fig. 4.

CLASS used as an input an approximate bounding box for the bladder. The box was defined manually using a Graphic User Interface (GUI) by drawing a bounding rectangle at a central slice where the bladder was the largest and by marking the top and the bottom slice that enclose the bladder. The process of defining the 3D bounding box is simple and fast. In those instances in which the bladder was partially filled with contrast material, the bounding box was split into two boxes—one enclosing the noncontrast-enhanced (NC) region and the other enclosing the contrast-filled (C) region of the bladder (Fig. 4). The splitting of the box was done also manually. The two boxes were defined to have an overlapping region at the transition between the C and NC regions. The time required to set the two boxes was negligible compared to manually outline the entire bladder. Following the above method the bounding boxes were defined efficiently over the bladder cases in the dataset. The splitting location between the contrast and noncontrast regions is not critical, as long as they overlap and do not cutoff one region or the other too early so that the two segmented volumes can overlap and be connected smoothly across the transition, as described below.

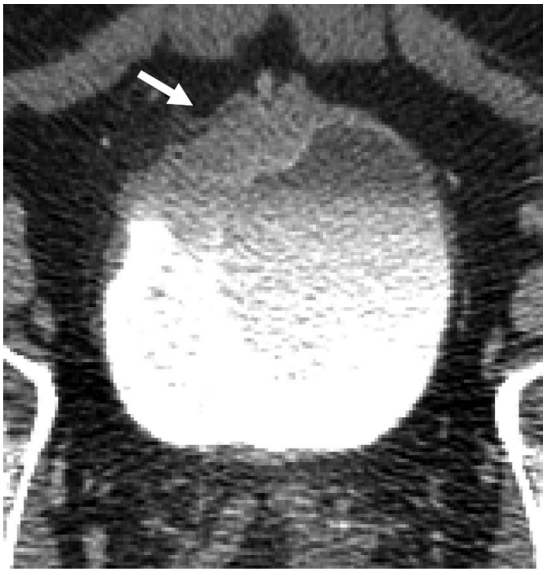

FIG. 3. Malignant lesion in the noncontrast part of the bladder (white arrow), which is partially filled with IV contrast.

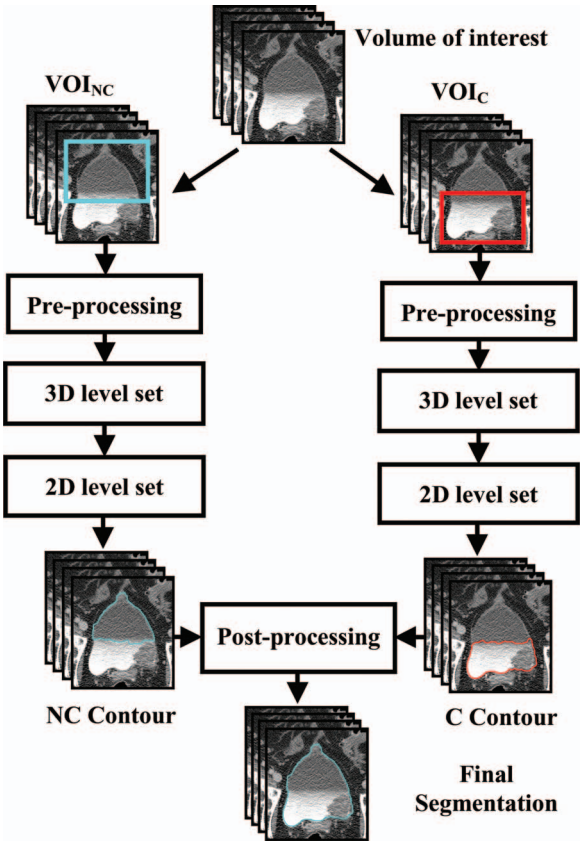

FIG. 4. Block diagram of the CLASS. Segmentation is performed separately in two 3D volumes of interest (VOIs); one contains the noncontrast (NC) region (VOI$_{NC}$), and the other the contrast-filled (C) region (VOI$_{C}$) of the bladder. The segmented contours of the NC and C regions are then combined into a complete contour of the bladder.

The NC and the C regions of the bladder were segmented in CLASS by applying stages 1, 2, and 3 separately to the predefined NC and C volumes of interest (VOI$_{NC}$ and VOI$_{C}$, respectively) (Fig. 4). Stages 1, 2, and 3 are functionally equivalent for both the VOI$_{NC}$ and VOI$_{C}$ branches in Fig. 4. CLASS is briefly described below. More details for stages 1, 2, and 3 can be found in the literature.[19]

In the first stage, preprocessing techniques are applied to the predefined volume of interest (VOI_{NC} or VOI_C) (Fig. 4) in the original 3D volume to obtain a set of smoothed images and a set of gradient images. Smoothing, anisotropic diffusion, gradient filters and rank transform of the gradient magnitude are used to generate a 3D edge image. The 3D edge image is used to generate the scalar speed term $P(\mathbf{x})$ and the vector field image $\mathbf{A}(\mathbf{x})$ used in the level set [see Eq. (1)]. A subset of voxels in the image is then selected based on attenuation, gradient, and location.[19] These procedures select a subset S of voxels that belong to smooth (low gradient) areas and are relatively close to the center of the lesion. The voxels in S are a statistical sample of the full population of voxels in the object of interest. The mean μ and standard deviation σ of the voxel values from the smoothed image within S are then computed. A subset of voxels that satisfy the criteria of falling within 3.0 standard deviations of the mean of the voxel values in S and with values above -400 HU is extracted from S. Morphological dilation filtering, 3D flood fill algorithm, and morphological erosion filtering are applied to this subset of voxels to connect neighboring components, fill holes, and extract an initial segmentation surface C.

In the second stage, the initial segmentation surface C is propagated using a 3D level set method.[19] Our chosen level set implementation evolves according to the equation:

$$\frac{\partial}{\partial t}\psi(\mathbf{x}) = -\alpha\mathbf{A}(\mathbf{x})\cdot\nabla\psi(\mathbf{x}) - \beta P(\mathbf{x})|\nabla\psi(\mathbf{x})| + \gamma\kappa(\mathbf{x})|\nabla\psi(\mathbf{x})|, \quad (1)$$

where α, β, and γ are the coefficients for the advection, propagation, and curvature terms, respectively, $\mathbf{A}(\mathbf{x})$ is a vector field image (assigning a vector to each voxel in the image) which drives the contour to move toward regions of high gradient, $P(\mathbf{x})$ is a scalar speed term between 0 and 1 causing the contour to expand at the local rate, and $\kappa(\mathbf{x}) = div\,(\nabla\psi(\mathbf{x})/|\nabla\psi(\mathbf{x})|)$ is the mean curvature of the level set at point $\mathbf{x}$. The symbol ∇ denotes the gradient operator and div is the divergence operator.

Three 3D level sets with predefined sets of parameters are applied in series to the initial contour C. The corresponding parameters of the three level sets are presented in Table I. The first level set slightly expands the initial contour and keeps it smooth. The second level set pulls the contour toward the sharp edges, but at the same time it expands slightly in regions of low gradient. The parameter "q" in Table I is defined to be a linear function $\sigma M + \phi$ of the 2D diagonal distance M of the VOI box in millimeters (mm), where $\sigma = 0.06$, $\phi = -0.11$ (based on our previous work[19]). Thus, larger VOIs will lead to larger γ for the second level set, and the curvature term of which will increase with the VOI diameter. Therefore, the level set will ignore fine inhomogeneities and focus more on the overall bladder shape when segmenting the bladder. The third level set further expands slightly the contour toward regions of low gradient.

TABLE I. Parameters for the bank of level sets.

Level set	α	β	γ	n
First	1.0	2.0	1.0	4
Second	1.0	0.4	q	150
Third	0	1.0	0	5
2D slices	4.0	0.3	0.5	400

In the third stage, a 2D level set is applied to every slice of the segmented object from the second stage. The 2D level set is allowed to propagate for a number of time steps in order to maintain a degree of interslice cohesion. The main purpose of the 2D level set is to refine the 3D contours at the top and the bottom of the object. The 3D level sets searched for the bladder surface using 3D information and constraints, which are more general and less prone to local noise and the 2D level set refined the 3D surface locally to make it more specific to local features.

In the fourth stage, a union operation is performed to combine the C and NC contours into the final contour.

In those cases in which the bladder is completely filled with contrast material or completely unenhanced, a single VOI, C or NC, will be defined to enclose the entire bladder and only the C or NC branch of CLASS without the fourth stage (Fig. 4) will be used for segmentation.

Examples of the CLASS segmentation of the partially filled bladders with contrast material from Figs. 2 and 3 are shown in Figs. 5 and 6, respectively. The segmented NC bladder regions are shown in Figs. 5(a) and 6(a), and the segmented C bladder regions are shown in Figs. 5(b) and 6(b). The final contours are shown in Figs. 5(c) and 6(c).

The cascaded 3D level sets and the 2D level set can guide the segmentation contour to go across the lesion boundaries within the bladder and correctly reach the bladder boundary. The first and the third 3D level sets tend to expand the contour toward regions of low gradient and go over some edges, which help propagate the contour over large or small lesions. The second 3D level set can ignore fine inhomogeneities and focus more on the overall bladder shape, which allows it to include small lesions within the segmented bladder contour while constraining against oversegmentation. We found experimentally that the specific functional order of the three 3D and the 2D level sets is important in order to successfully handle various bladder shapes with various lesions of different sizes, shapes and contrasts, as shown in the examples in Sec. 3.

2.B. Bladder segmentation using ITK-SNAP

For comparison purpose, the bladders were also segmented by using ITK-SNAP 2.4,[18] which is a publicly available open source software application used to segment structures in 3D medical images. The segmentation was performed by using the edge-based level sets (snakes). The approximate bounding box for the bladder was used as the required input for the ITK-SNAP segmentation. The preprocessing included Gaussian blurring, edge contrast, and edge mapping exponent. The level sets were initialized by a sphere placed inside the object being segmented. ITK sparse field level set algorithm was used to guide the contour propagation. After experimentation

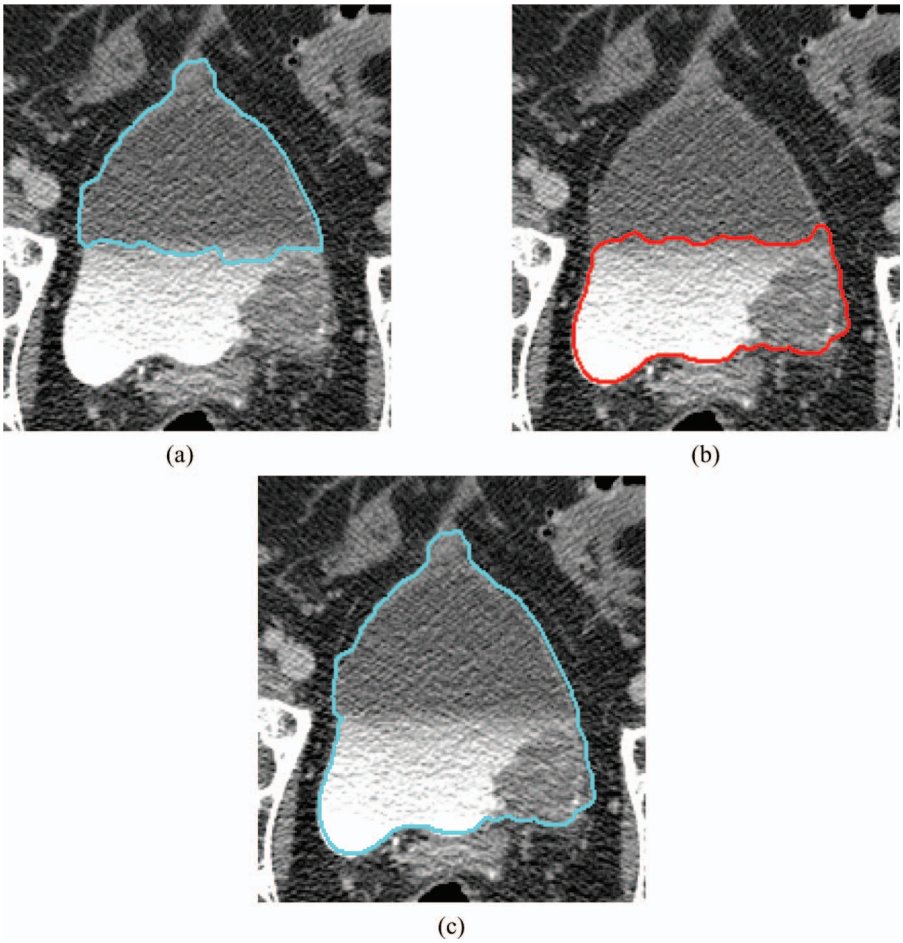

FIG. 5. Bladder segmentation using CLASS: (a) segmentation of the noncontrast-enhanced (NC) portion of the bladder (highlighted contour); (b) segmentation of the contrast-enhanced (C) portion of the bladder (highlighted contour); and (c) entire bladder segmentation (highlighted contour) is then obtained from the union of the NC contour (a) and C contour (b). The same bladder, without the segmented contour, is shown in Fig. 2.

with the bladder cases, the coefficients for the advection, propagation, and curvature terms of the level set were chosen to be the values shown in Table II. The number of level set iterations was set to be 4500, where in general convergence was observed. The radius of the initial sphere was set to be $\frac{1}{4}$ of the smallest sidelength of the 3D bounding box. The sphere was manually placed at the boundary between the C and NC parts of the bladders with C and NC regions, and in the middle of the bladders that had only C or NC region.

2.C. Data set

In this study, a data set of 81 patients undergoing CTU who subsequently underwent cystoscopy and biopsy was utilized. The cases were collected retrospectively from the Abdominal Imaging Division of the Department of Radiology at the University of Michigan with approval of the Institutional Review Board. Of the 81 bladders, 40 bladders contained focal mass-like lesions (32 malignant and 8 benign), 26 bladders had wall thickening (20 malignant and 6 benign) and 15 were normal. Sixty one bladders were partially filled with excreted contrast material, eight were completely filled with excreted contrast material, and 12 had no visible excreted contrast material. The bladder conspicuity was medium to high.

The MDCT urography scans used in this study were acquired with GE Healthcare LightSpeed MDCT scanners. Excretory phase images, obtained 12 min after the initiation of the first bolus of a split-bolus intravenous contrast injection and 2 min after the initiation of the second bolus of 175 ml of nonionic contrast material at a concentration of 300 mg iodine per ml, were utilized. The images used were acquired at an interval and slice thickness of 1.25 mm using 120 kVp and 120–280 mA. Since patients were not turned prior to image acquisition, dependently layering IV contrast material that had been excreted into the renal collecting systems partially filled the bladder on the CTU images.

2.D. Evaluation methods

The performance of the segmentation was evaluated by a quantitative and a qualitative method. For the quantitative assessment, an experienced radiologist provided manual outlines on the CT slices for a random subset of 30 of the 81 bladders using a graphic user interface (GUI). The radiologist outlined the bladder on every 2D CT slice on which the

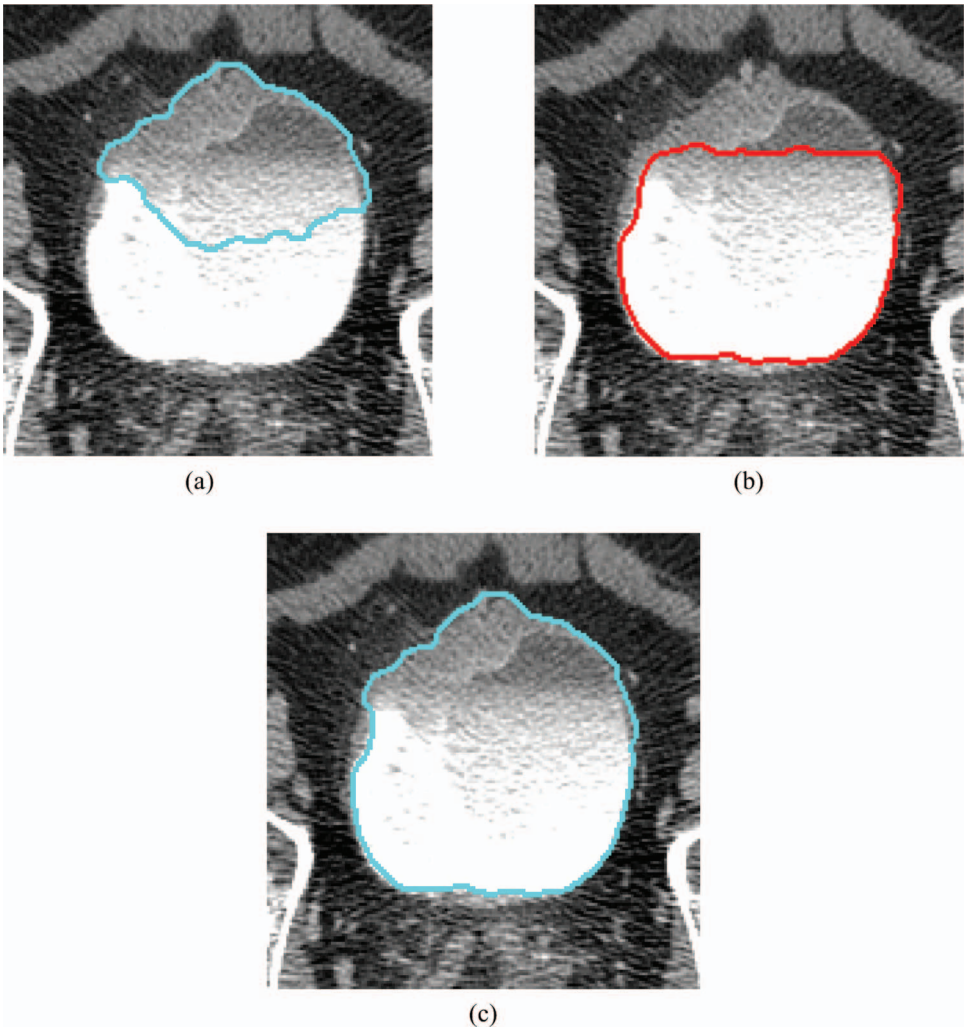

FIG. 6. Bladder segmentation using CLASS: (a) segmentation of the noncontrast-enhanced (NC) portion of the bladder (highlighted contour); (b) segmentation of the contrast-enhanced (C) portion of the bladder (highlighted contour); and (c) entire bladder segmentation (highlighted contour) is then obtained from the union of the NC contour (a) and C contour (b). The same bladder, without the segmented contour, is shown in Fig. 3.

bladder was visible, resulting in a 3D surface contour. There were a total of 2904 slices manually outlines by the radiologist for the 30 bladders. Several different performance metrics[19–21] that quantify the similarity of a pair of contours were used for evaluating the system, including the average distance, the volume intersection ratio, the volume error between the radiologist contours, and CLASS segmented contours and the Jaccard index.[22] The average distance between two 3D surface contours G and U is defined as

$$\mathrm{AVDIST}(G,U) = \frac{1}{2}\left(\frac{\sum_{x\in G}\min\{d(x,y) : y \in U\}}{N_G} + \frac{\sum_{y\in U}\min\{d(x,y) : x \in G\}}{N_U}\right), \quad (2)$$

TABLE II. Parameters for the ITK-SNAP level set.

Level set	α	β	γ	n
ITK-SNAP	3.5	0.4	0.17	4500

where G is the gold standard 3D surface contour marked by the radiologist and U is the 3D contour being evaluated. N_G and N_U denote the number of points (voxels) on G and U, respectively. The function d is the Euclidean distance. For a given voxel along the contour G, the distance to the closest point along the contour U is determined. The minimum distances obtained for all points in G are averaged. This process is repeated by switching the roles of G and U. The two average minimum distances are then averaged.

The volume intersection ratio is defined as the ratio of the intersection between the gold standard volume and the segmented volume to the gold standard volume:

$$R^{3D} = \frac{V_G \cap V_U}{V_G}, \quad (3)$$

where V_G is the volume enclosed by the gold standard contour G and V_U is the volume enclosed by the contour U. A value of 1 indicates that V_U completely overlaps with V_G, whereas a value of 0 implies V_U and V_G are disjoint.

The volume error is defined as the ratio of the difference between the two volumes to the gold standard volume, i.e.,

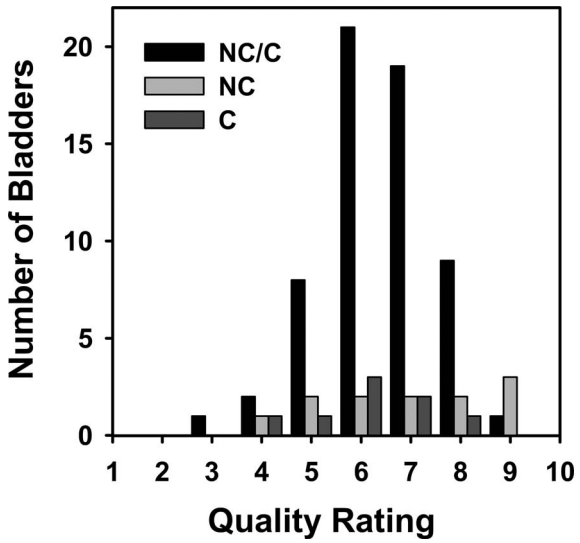

FIG. 7. Histogram for the quality ratings of the CLASS segmented contours: 61 bladders partially filled with excreted contrast material (NC/C) with average segmentation quality rating of 6.4; 12 bladders which did not contain any excreted contrast material (NC) with average quality rating of 6.9; eight bladders completely filled with excreted contrast material (C) with average quality rating of 6.1.

$$E^{3D} = \frac{V_G - V_U}{V_G}, \tag{4}$$

where negative error indicates oversegmentation and vice versa. Because the over- and undersegmentation tend to mask the actual deviations from the gold standard when the average is taken, the absolute (unsigned) error $|E^{3D}|$ is also calculated.

The Jaccard index is defined as the ratio of the intersection between the gold standard volume and the segmented volume to the union of the gold standard volume and the segmented volume:

$$JACCARD^{3D} = \frac{V_G \cap V_U}{V_G \cup V_U}, \tag{5}$$

A value of 1 indicates that V_U completely overlaps with V_G, whereas a value of 0 implies V_U and V_G are disjoint.

Note that there is no single measure that can describe completely the agreement between the two volumes. However, by combining two performance measures, one can derive a number of performance measures that can assess different aspects of the performance; for example, the Jaccard index, the overlap and nonoverlap fractions with the gold standard, can be derived from the volume intersection ratio and the volume error.[21]

Because of the extensive effort required to manually outline each bladder, which on average amounted to 94 slices (range: 32–161 slices) in the CTU scan, we obtained the reference standards for quantitative evaluation only for a subset

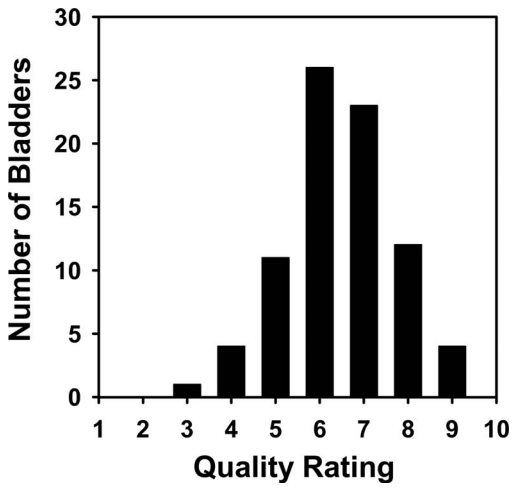

FIG. 8. Histogram for the quality ratings of the 81 CLASS segmented contours with an average quality rating of 6.5.

of the 81 bladders. A qualitative assessment was performed to evaluate the segmentation of the entire data set by CLASS. The quality of each 3D contour was visually judged by overlaying the computer-segmented 3D contour on the CT images slice by slice on the display workstation. The overall closeness of the 3D contour to the bladder boundary was rated on a scale from 1 to 10 (1 = "very poor," 2 = "poor," 5 = "fair," 7 = "good," 9 = "excellent," 10 = "perfect").

3. RESULTS

Examples of the CLASS segmentation of two bladders with a segmentation quality rating of 8 are shown in Figs. 5 and 6. For the 61 bladders partially filled with excreted contrast material (NC/C), the average quality rating for the CLASS segmented contours was 6.4 ± 1.1 (Fig. 7). Twenty nine of the contours were given quality ratings of 7 or above. Only three contours were given a rating under 5 ("fair"). For the eight bladders completely filled with excreted contrast material (C) or the 12 that did not contain any excreted contrast material (NC), the average quality ratings were 6.1 ± 1.2 and 6.9 ± 1.7, respectively (Fig. 7). Only 1 NC and 1 C contour were given a rating of 4. For the entire set of 81 bladders, the average quality rating of the CLASS segmentation was 6.5 ± 1.3 (Fig. 8). Thirty nine bladders were given quality ratings of 7 or above. Only five bladders had ratings under 5.

For the subset of 30 bladders randomly selected for quantitative analysis, the average quality rating of the CLASS segmentation was 6.4 ± 0.9. The segmentation results averaged over 30 bladders are presented in Table III. Figure 9 shows

TABLE III. Segmentation results for CLASS and ITK-SNAP, averaged over the subset of 30 bladders randomly selected for quantitative analysis.

Segmentation method	R^{3D}	E^{3D}	$\|E^{3D}\|$	AVDIST (mm)	$JACCARD^{3D}$
CLASS	(79.0 ± 8.2)%	(16.1 ± 16.3)%	(19.9 ± 11.1)%	3.5 ± 1.3	(75.7 ± 8.4)%
ITK-SNAP	(78.8 ± 16.3)%	(8.3 ± 33.1)%	(24.2 ± 23.7)%	5.2 ± 2.6	(71.0 ± 15.4)%

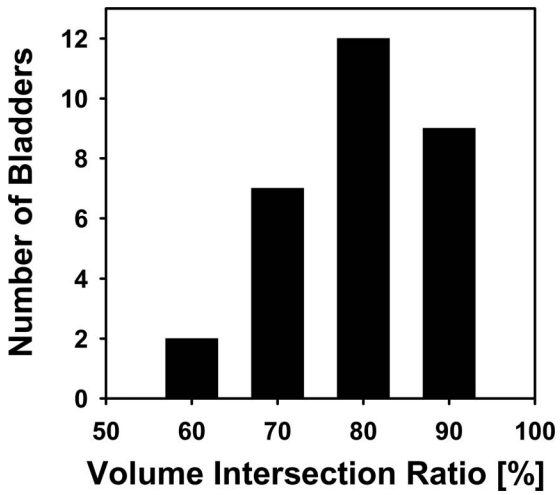

FIG. 9. Histogram of the volume intersection ratio R^{3D}. The average was 79.0%.

the histogram of the volume intersection ratios, R^{3D}. Twenty two bladders had R^{3D} higher than 75%. The histogram of the volume errors, E^{3D}, is shown in Fig. 10. Eleven bladders had an absolute volume error $|E^{3D}|$ smaller than 15%. Fourteen of the bladders had an average distance measure, AVDIST of less than 3 mm (Fig. 11). Eighteen bladders had $JACCARD^{3D}$ higher than 75%.

The ITK-SNAP segmentation results averaged over the 30 bladders are also presented in Table III. The performance measures of ITK-SNAP segmentation were consistently inferior to that of CLASS. In comparison to ITK-SNAP, the CLASS segmentation yield smaller average distance error, smaller absolute error, larger $JACCARD^{3D}$ and smaller standard deviations for all the measures. However, only the AVDIST difference between ITK-SNAP and CLASS was statistically significant ($p < 0.001$ by two-tailed paired t-test).

Additional examples of the CLASS and the ITK-SNAP segmented bladders are shown in Figs. 12 and 13. The segmentation quality ratings of these examples are based on CLASS segmentation and range from the best (9) to the

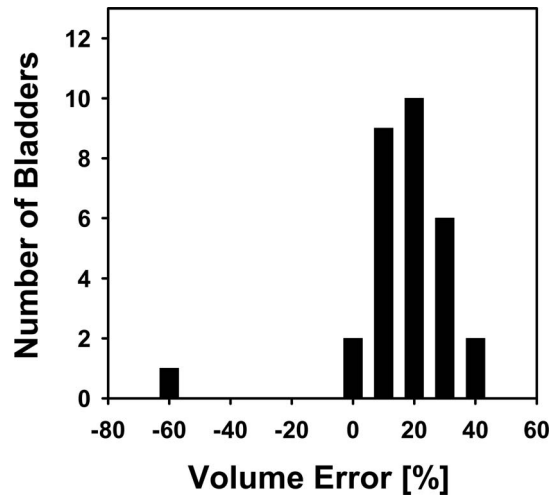

FIG. 10. Histogram of the volume error E^{3D}. The average was 16.1%.

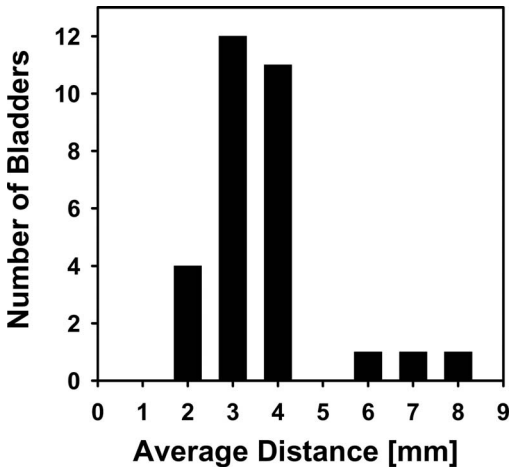

FIG. 11. Histogram of the average distance measure *AVDIST*. The average was 3.5 mm.

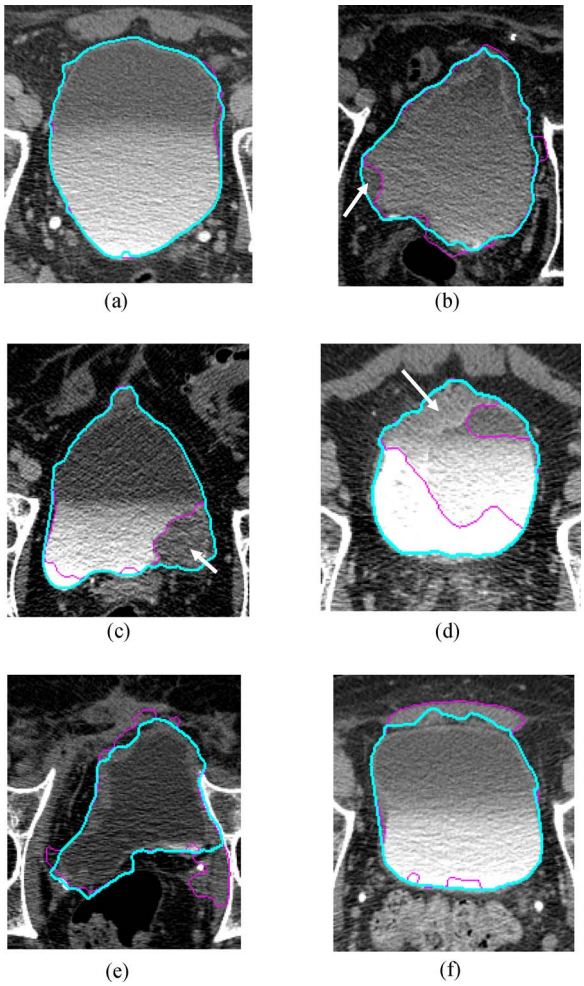

FIG. 12. Bladder segmentations using CLASS (highlighted bold contour) and ITK-SNAP (highlighted thin contour). The segmentation quality ratings are based on the CLASS segmentation: (a) bladder partially filled with contrast material (NC/C) with quality rating of 9; (b) bladder filled with very small amount of contrast (almost NC) with quality rating of 9; (c) NC/C bladder with quality rating of 8 (the same bladder, without the segmented contour, is shown in Fig. 2); (d) NC/C bladder with quality rating of 8 (the same bladder, without the segmented contour, is shown in Fig. 3); (e) bladder without contrast (NC) with quality rating of 8; (f) NC/C bladder with quality rating of 7. The white arrows point to the bladder lesions.

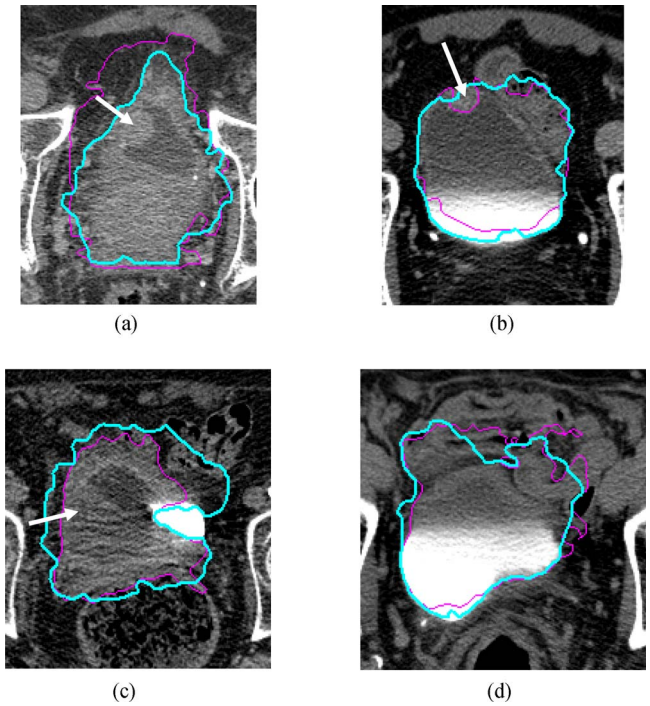

FIG. 13. Bladder segmentations using CLASS (highlighted bold contour) and ITK-SNAP (highlighted thin contour). The segmentation quality ratings are based on the CLASS segmentation: (a) NC bladder with quality rating of 6; (b) NC/C bladder with quality rating of 5; (c) bladder with small amount of contrast material with the quality rating of 4; (d) NC/C bladder with quality rating of 3. The white arrows point to the bladder lesions.

worst (3) ratings in our data set (Figs. 7 and 8, respectively). The contours in Fig. 12 cover a quality rating range of 7–9. The contours in Fig. 13 cover a quality rating range of 3–6. Figure 13(d) shows the segmentation result of the only bladder with a segmentation quality rating of 3.

4. DISCUSSION

In this study, our CLASS segmentation system was applied to a data set containing bladders in CTUs having a wide range of image quality. Most of the bladders were partially filled with excreted contrast material. However, some bladders were entirely filled with excreted contrast material and others did not contain any contrast-enhanced urine. Our segmentation system performed well for the variety of bladder images with different degrees of contrast opacification, different shapes, different sizes, and different abnormalities [Figs. 5, 6, 12, and 13(a)]. About half of the bladder segmentations were given quality ratings of 7 ("good") or above. CLASS was able to segment successfully the majority of both the NC and C bladders. The NC bladder contours had the highest number of segmentation quality ratings of 9 ("excellent"). More than 70% of the bladders with manual outlines had large volume intersection ratio ($R^{3D} > 75\%$) (Fig. 9), 60% had large Jaccard index ($JACCARD^{3D} > 75\%$), and about half had small average distance measure (AVDIST < 3 mm) (Fig. 11). A bladder with a large malignant lesion within the contrast-enhanced area was successfully segmented [Fig. 5(c)]. Another bladder with a malignant lesion in the noncontrast part of the bladder and partially filled with contrast material was also segmented successfully [Fig. 6(c)]. Even though the bladders in Figs. 12(e) and 13(a) did not contain IV contrast material, had irregular shapes, and most of the boundaries between the bladders and the adjacent normal tissues were of very low contrast, the CLASS segmented contours were considered to be reasonable.

There were cases for which the CLASS method did not produce good contours. For example, the bladders in Figs. 13(b)–13(d) were oversegmented. The low quality of the segmentation may be attributed to the very low contrast between the bladders and the surrounding complex background of perivesical tissue, especially when loops of bowel were located directly adjacent to the bladder [Fig. 13(b)]. The bladder in Fig. 13(c) was also undersegmented, with the small contrast-containing area being excluded. Due to the strong gradient at the location where the bladder without contrast bordered the dense contrast-containing portion of the bladder, the segmentation system in this instance excluded the contrast-enhanced portion and was not able to find the correct bladder boundary.

CLASS is not fully automated and requires the placement of two bounding boxes for the contrast and noncontrast regions of the bladder. The placement of the boxes needs minimal effort and is much more efficient than manual segmentation of the 32 to 161 slices of the bladder following the irregular boundaries. The CLASS segmentation offers a practical way for further quantitative analysis of bladder abnormalities. The segmentation results may depend on the bounding box locations and sizes to a certain extent. The dependence may be stronger for the cases with very irregular bladder boundary, especially when the CT values of the adjacent tissue are very similar to that of the bladder where the chance of segmentation leak is high.

The ITK-SNAP segmentations achieved varied levels of accuracy. In a number of cases the segmentation was good as shown in Fig. 12(a). The segmentation of the bladder in Fig. 13(c), which is a difficult case, was better with ITK-SNAP than with CLASS. However, there are a number of cases, for which ITK-SNAP oversegmented the bladders as shown in Figs. 12(e) and 12(f) and Figs. 13(a) and 13(d), or undersegmented the bladders as shown in Figs. 12(c) and 12(d) and Fig. 13(b). In most of the cases the contrast part of the bladder was undersegmented as seen in Figs. 12(c) and 12(d), and 12(f) and Figs. 13(b)–13(d) due to the steep, rapid change of the gray level intensity. The ITK-SNAP also tended to exclude lesions as shown in Figs. 12(b) and 12(c) and Fig. 13(b) again due to due to rapid change of the gray level intensity at the lesion location.

This pilot study has several limitations. One limitation is the relatively small data set. A second limitation is that the number of manual 3D bladder outlines was also relatively small, although this study already has the largest data set among those in the literature. Another limitation is that the CLASS method was not able to reliably stop the contour at the bladder boundary when a complex background is present. Better criteria to prevent leakage into adjacent normal

tissue across low contrast boundaries are needed. It may also be necessary to develop additional local refinement methods to improve segmentation accuracy. We are in a process of collecting a larger database to further improve the bladder segmentation method, and also collecting additional manual outlines for more reliable quantitative evaluation of the performance of CLASS.

5. CONCLUSION

The preliminary results demonstrate the feasibility of the CLASS for the segmentation of bladders on CTU scans. CLASS performs segmentation of the contrast and noncontrast filled regions of the bladder separately to overcome the large difference in the CT intensities of the two regions, and uses a combination of 3D and 2D level sets to achieve initial segmentation and refinement. Further study is underway to improve and evaluate quantitatively the segmentation performance with a larger data set and a larger number of manual bladder outlines to be used as a reference standard. This study is the first step toward the development of a reliable and efficient system for segmentation of bladders, which is a critical component of a CAD system for detection of malignant and benign urothelial lesions imaged with CT urography.

ACKNOWLEDGMENT

This work is supported by USPHS Grant R01CA134688.

[a]Author to whom correspondence should be addressed. Electronic mail: lhadjisk@umich.edu; Telephone: (734) 647-7428; Fax: (734) 615-5513.

[1]American Cancer Society, "Cancer Facts & Figures 2012" (2012) (available URL: www.cancer.org).
[2]C. L. McCarthy and N. C. Cowan, "Multidetector CT urography (MDCTU) for urothelial imaging," Radiology (P) **225**, 237 (2002).
[3]M. Noroozian, R. H. Cohan, E. M. Caoili, N. C. Cowan, and J. H. Ellis, "Multislice CT urography: State of the art," Br. J. Radiol. **77**, 74–86 (2004).
[4]S. A. Akbar, K. J. Mortele, K. Baeyens, M. Kekelidze, and S. G. Silverman, "Multidetector CT urography: Techniques, clinical applications, and pitfalls," Semin. Ultrasound CT MR **25**, 41–54 (2004).
[5]W. C. Liu, K. J. Mortele, and S. G. Silverman, "Incidental extraurinary findings at MDCT urography in patients with hematuria: Prevalence and impact on imaging costs," Am. J. Roentgenol. **185**, 1051–1056 (2005).
[6]E. M. Caoili, R. H. Cohan, M. Korobkin, J. F. Platt, I. R. Francis, G. J. Faerber, J. E. Montie, and J. H. Ellis, "Urinary tract abnormalities: Initial experience with multi-detector row CT urography," Radiology **222**, 353–360 (2002).
[7]G. S. Sudakoff, D. P. Dunn, M. L. Guralnick, R. S. Hellman, D. Eastwood, and W. A. See, "Multidetector computerized tomography urography as the primary imaging modality for detecting urinary tract neoplasms in patients with asymptomatic hematuria," J. Urol. **179**, 862–867 (2008).
[8]S. B. Park, J. K. Kim, H. J. Lee, H. J. Choi, and K.-S. Cho, "Hematuria: Portal venous phase multi detector row CT of the bladder–a prospective study," Radiology **245**, 798–805 (2007).
[9]L. Li, Z. Wang, X. Li, X. Wei, H. L. Adier, W. Huang, S. Rizvi, H. Meng, D. P. Harrington, and Z. Liang, "A new partial volume segmentation approach to extract bladder wall for computer aided detection in virtual cystoscopy," Proc. SPIE **5369**, 199–206 (2004).
[10]C. Duan, Z. Liang, S. Bao, H. Zhu, S. Wang, G. Zhang, J. J. Chen, and H. Lu, "A coupled level set framework for bladder wall segmentation with application to MR cystography," IEEE Trans. Med. Imaging **29**, 903–915 (2010).
[11]C. J. Duan, K. H. Yuan, F. H. Liu, P. Xiao, G. Q. Lv, and Z. R. Liang, "Volume-based features for detection of bladder wall abnormal regions via MR cystography," IEEE Trans. Biomed. Eng. **58**, 2506–2512 (2011).
[12]C. J. Duan, K. H. Yuan, F. H. Liu, P. Xiao, G. Q. Lv, and Z. R. Liang, "An adaptive window-setting scheme for segmentation of bladder tumor surface via MR cystography," IEEE Trans. Inf. Technol. Biomed. **16**, 720–729 (2012).
[13]Q. Song, X. D. Wu, Y. L. Liu, M. Smith, J. Buatti, and M. Sonka, "Optimal graph search segmentation using arc-weighted graph for simultaneous surface detection of bladder and prostate," in *Medical Image Computing and Computer-Assisted Intervention - MICCAI 2009, Part II, Proceedings*, edited by G. Z. Yang, D. Hawkes, D. Rueckert, A. Nobel, and C. Taylor (Springer-Verlag, Berlin, 2009).
[14]X. F. Chai, M. van Herk, A. Betgen, M. Hulshof, and A. Bel, "Automatic bladder segmentation on CBCT for multiple plan ART of bladder cancer using a patient-specific bladder model," Phys. Med. Biol. **57**, 3945–3962 (2012).
[15]X. F. Chai, M. van Herk, M. Hulshof, and A. Bel, "A voxel-based finite element model for the prediction of bladder deformation," Med. Phys. **39**, 55–65 (2012).
[16]L. M. Hadjiiski, B. Sahiner, H. P. Chan, E. M. Caoili, R. H. Cohan, and C. Zhou, "Automated segmentation of urinary bladder and detection of bladder lesions in multi-detector row CT urography," Proc. SPIE **7260**, 72603R (2009).
[17]L. Hadjiiski, H. P. Chan, Y. Law, R. H. Cohan, E. M. Caoili, H. C. Cho, C. Zhou, and J. Wei, "Segmentation of urinary bladder in CT urography (CTU) using CLASS," Proc. SPIE **8315**, 83150J (2012).
[18]P. A. Yushkevich, J. Piven, H. C. Hazlett, R. G. Smith, S. Ho, J. C. Gee, and G. Gerig, "User-guided 3D active contour segmentation of anatomical structures: Significantly improved efficiency and reliability," Neuroimage **31**, 1116–1128 (2006).
[19]E. Street, L. Hadjiiski, B. Sahiner, S. Gujar, M. Ibrahim, S. K. Mukherji, and H. P. Chan, "Automated volume analysis of head and neck lesions on CT scans using 3D level set segmentation," Med. Phys. **34**, 4399–4408 (2007).
[20]B. Sahiner, N. Petrick, H. P. Chan, L. M. Hadjiiski, C. Paramagul, M. A. Helvie, and M. N. Gurcan, "Computer-aided characterization of mammographic masses: Accuracy of mass segmentation and its effects on characterization," IEEE Trans. Med. Imaging **20**, 1275–1284 (2001).
[21]T. W. Way, L. M. Hadjiiski, B. Sahiner, H.-P. Chan, P. N. Cascade, E. A. Kazerooni, N. Bogot, and C. Zhou, "Computer-aided diagnosis of pulmonary nodules on CT scans: Segmentation and classification using 3D active contours," Med. Phys. **33**, 2323–2337 (2006).
[22]P. Jaccard, "The distribution of the flora in the alpine zone," New Phytol. **11**, 37–50 (1912).